Journal of Magnetic Resonance **145,** 192–200 (2000)
doi:10.1006/jmre.2000.2120, available online at http://www.idealibrary.com on IDEAL®

# Separation of Anisotropy and Exchange Broadening Using $^{15}$N CSA–$^{15}$N–$^{1}$H Dipole–Dipole Relaxation Cross-Correlation Experiments

Christian Renner and Tad A. Holak

*Max Planck Institute for Biochemistry, 82152 Martinsried, Germany*

Received August 4, 1999; revised May 1, 2000

**Based on the measurement of cross-correlation rates between $^{15}$N CSA and $^{15}$N–$^{1}$H dipole–dipole relaxation we propose a procedure for separating exchange contributions to transverse relaxation rates ($R_2 = 1/T_2$) from effects caused by anisotropic rotational diffusion of the protein molecule. This approach determines the influence of anisotropy and chemical exchange processes independently and therefore circumvents difficulties associated with the currently standard use of $T_1/T_2$ ratios to determine the rotational diffusion tensor. We find from computer simulations that, in the presence of even small amounts of internal flexibility, fitting $T_1/T_2$ ratios tends to underestimate the anisotropy of overall tumbling. An additional problem exists when the N–H bond vector directions are not distributed homogeneously over the surface of a unit sphere, such as in helix bundles or $\beta$-sheets. Such a case was found in segment 4 of the gelation factor (ABP 120), an F-actin cross-linking protein, in which the diffusion tensor cannot be calculated from $T_1/T_2$ ratios. The $^{15}$N CSA tensor of the residues for this $\beta$-sheet protein was found to vary even within secondary structure elements. The use of a common value for the whole protein molecule therefore might be an oversimplification. Using our approach it is immediately apparent that no exchange broadening exists for segment 4 although strongly reduced $T_2$ relaxation times for several residues could be mistaken as indications for exchange processes.** © 2000 Academic Press

*Key Words:* **$^{15}$N NMR relaxation; spectral density mapping; $^{15}$N chemical shift anisotropy; anisotropic rotational diffusion; cross-correlation.**

## INTRODUCTION

Increasingly it is being recognized that $^{15}$N relaxation studies can contribute to our understanding of protein dynamics, protein stability and function, and protein–ligand interactions with information that is not available from any other technique (*1–4*). However, protein motions on time scales of micro- to milliseconds are difficult to assess with standard $^{15}$N relaxation measurements, i.e., longitudinal $T_1$, transverse $T_2$, and heteronuclear $^{15}$N{$^{1}$H} NOE experiments (*2–5*). These experiments provide information mainly on thermal fluctuations on the picosecond to nanosecond time scales. In principle, the Lipari–Szabo model (*6, 7*) provides also means for extracting exchange broadening contributions from processes on the micro- to millisecond time scales (*8*). However, if anisotropy of the rotational diffusion is not incorporated correctly, exchange contribution estimates will be inaccurate (*9*). In most practical cases it is difficult to determine the diffusion tensor and N–H bond vector directions (with respect to the diffusion tensor) for a molecule in solution independently from the relaxation data. We performed tests on large simulated synthetic data sets that indicate that fitting the diffusion tensor to experimental $T_1/T_2$ ratios tends to underestimate the anisotropy when internal flexibility or exchange broadening is present, even if these contributions are only small. There are currently experimental schemes described that aim at the direct quantification of exchange broadening (*10–12*). Unfortunately only a quite small range of time scales is accessible through these $T_{1\rho}$ or $T_2$ experiments. Also precision of the results is limited for moderately concentrated protein samples (*13*).

Recently, Tjandra *et al.* (*14*) and Tessari *et al.* (*15*) developed NMR experiments that allow measurements of transverse cross-correlation rates between the $^{15}$N CSA and the $^{15}$N–$^{1}$H dipole–dipole relaxation. We propose here to apply these experiments to distinguish contributions to the transverse relaxation rates from exchange broadening and from anisotropic overall rotation. Kroenke *et al.* (*16*) have already published a method for separating these contributions to the transverse relaxation rates using two additional experiments, one a slight modification of the experiment developed by Tjandra *et al.* (*14*), and the other designed to measure the longitudinal cross-correlation rate between the $^{15}$N CSA and the $^{15}$N–$^{1}$H dipole–dipole relaxation. We show here that a single experiment that measures the transverse cross-correlation rate is already sufficient for this purpose. An additional advantage of incorporating one of these highly sensitive and straightforward experiments into the standard set of relaxation experiments is the ability to calculate the $^{15}$N CSA for each observed residue if data from at least two fields are available (*17, 18*). Analysis of the data, with either Lipari–Szabo models or the reduced spectral density approach, can then be performed with residue-specific values for the $^{15}$N CSA. The usefulness and ease of this approach are demonstrated on segment 4 of the gelation factor (ABP 120), an F-actin cross-linking protein that contains solely $\beta$-sheets (*19*).



1090-7807/00 $35.00

## RESULTS

The cross-correlation rate $\eta$ between $^{15}$N CSA and $^{15}$N–$^{1}$H dipole–dipole relaxation is given by the following combination of spectral density values $J(\omega)$,

$$\eta = dc[4J(0) + 3J(\omega_N)]P_2(\cos\theta), \quad [1]$$

with $c$ and $d$ as in (*17*): $c = \gamma_N B_0(\sigma_\parallel - \sigma_\perp)/3$, $d = -(\mu_0/(4\pi))\gamma_H\gamma_N h/(4\pi r_{NH}^3)$ ($d^2 \approx 1.3\ 10^9\ s^{-2}$, $c^2 \approx 0.29\ 10^9\ s^{-2}$ at 500 MHz proton frequency), where symbols have their usual meanings and $P_2(x) = (3x^2 - 1)/2$ is the second-rank Legendre polynomial; $\theta$ is the angle between the $^{15}$N–$^{1}$H bond vector and the principal axis of the $^{15}$N chemical shift tensor, assumed axially symmetric. $\sigma_\parallel - \sigma_\perp$ is the chemical shift anisotropy of the amide $^{15}$N; $\omega_i$ denotes the resonance frequency of nucleus $i$ in the static magnetic field. The similarity of Eq. [1] to the expression for the transverse relaxation rate $R_2$

$$R_2 = (d^2 + c^2)/2[4J(0) + 3J(\omega_N)] + d^2/2[J(\omega_H - \omega_N) + 6J(\omega_H) + 6J(\omega_H + \omega_N)] \quad [2]$$

will be exploited below to determine $2dc/(c^2 + d^2)P_2(\cos\theta)$ (*17*).

Figures 1A and 1B show a comparison of cross-correlation rates $\eta_a$ and $\eta_b$ for segment 4 at two temperatures, 34 and 40°C, where $\eta_a$ and $\eta_b$ were obtained with the experiments proposed by Tjandra *et al.* (*14*) and Tessari *et al.* (*15*), respectively. Because the two experiments use different strategies to measure the same cross-correlation rate good agreement can serve as a check not only for precision but also for accuracy of the data. Included in Fig. 1C are also cross-correlation rates at two additional temperatures, 20 and 31°C, obtained with the Tjandra (*14*) and Tessari (*15*) experiments, respectively. We find the experiment of Tessari *et al.* (*15*) preferable as it is easier to extract the cross-correlation rates from spectra and requires no additional pulses for the cross-correlation experiment compared to the reference experiment (see Experimental). Also in our case the Tessari experiment (*15*) was slightly superior in sensitivity (approx 5–10%) compared to the Tjandra experiment (*14*) when using the same setup, especially the same time during which cross-correlation is active. The dependence of $\eta$ on temperature (through the overall tumbling rate) is readily visible in Fig. 1. The contributions from internal motions are expected to change even more dramatically with temperature (*2*). Anisotropy of the overall tumbling leads to variation of $\eta$ (dependent on the N–H bond direction) that does not depend on temperature. It is important to keep in mind that exchange broadening does not change $\eta$ as it affects cross-correlation and the reference experiment equally. These different properties of $\eta$ and $R_2$ can be utilized to identify exchange contributions.

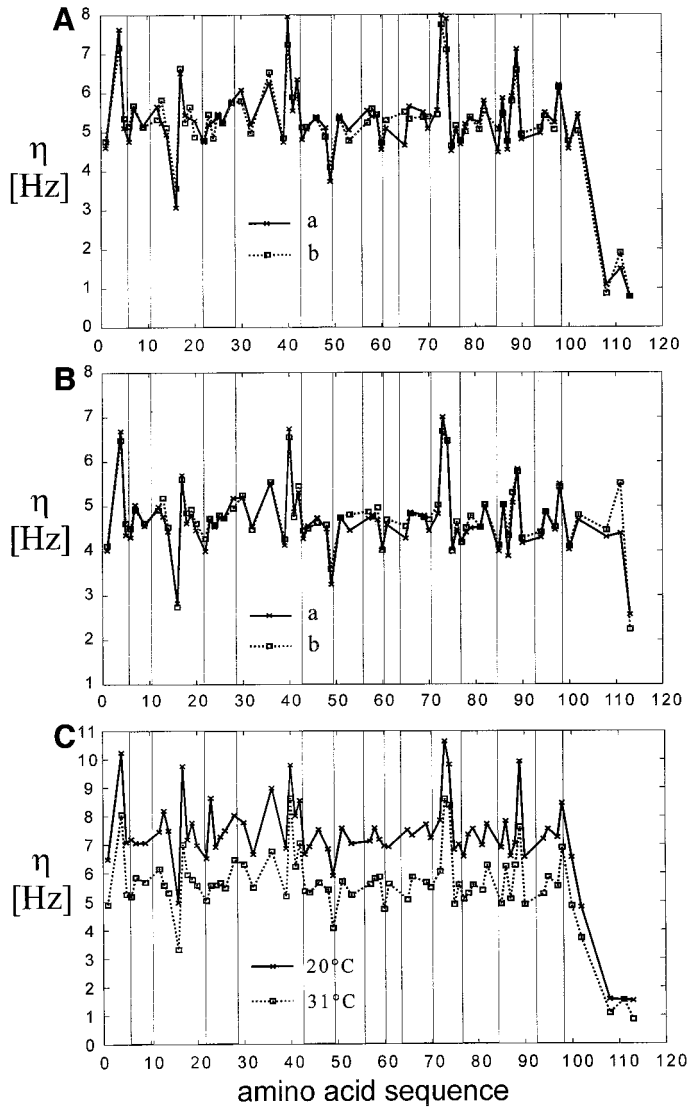


**FIG. 1.** Plot of the cross-correlation rates $\eta$ between $^{15}$N CSA and $^{15}$N–$^{1}$H dipole–dipole relaxation vs sequence for segment 4. The rates of panels A and B were determined at 34 and 40°C, respectively, from spectra recorded at 500 MHz proton frequency. Curves a and b correspond to rates measured with the experiments of Tjandra *et al.* (*14*) and Tessari *et al.* (*15*), respectively. Panel C shows cross-correlation rates at two additional temperatures, 20 and 31°C. The $\beta$-sheets of segment 4 are indicated by the shaded bars.

The reduced spectral density approach is used to calculate $J(0)$, $J(\omega_N)$, and $J(0.87\ \omega_H)$ from a standard set of $T_1$, $T_2$, and heteronuclear NOE (*20*). With $\eta$ and $J(\omega_N)$ values of the spectral density function at $\omega = 0$, $J^{cc}(0)$ values that are free from exchange contributions can be calculated using Eq. [1] ($J^{cc}(0)$ indicates the origin from the cross-correlation rate). Comparison of $J(0)$ and $J^{cc}(0)$ directly yields the exchange contribution. For residues with high NOE values and therefore low $J(0.87\ \omega_H)$ the residual variation of $J^{cc}(0)$ over the sequence must be caused by anisotropy, neglecting possible differences in CSA for the moment. The influence of residue-

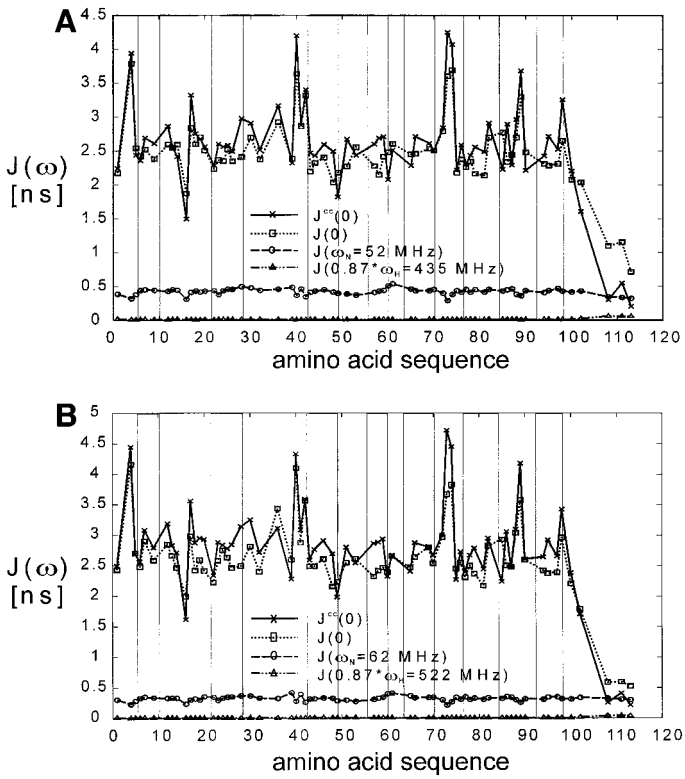


**FIG. 2.** Panels A and B show plots of $J^{cc}(0)$, $J(0)$, $J(\omega_N)$, and $J(0.87\ \omega_H)$ for segment 4 at 31°C from 500-MHz and 600-MHz data, respectively. The $\beta$-sheets of segment 4 are indicated by the shaded bars.

specific CSA on $J^{cc}(0)$ and on subsequent determination of anisotropy is discussed at the end of this section. Figures 2A and 2B show plots of $J^{cc}(0)$, $J(0)$, $J(\omega_N)$, and $J(0.87\ \omega_H)$ for segment 4 at 31°C from 500- and 600-MHz data, respectively. It can immediately be seen that no significant exchange broadening exists for segment 4 at this temperature. The mean difference between $J^{cc}(0)$ and $J(0)$ for the folded part of the protein is 0.07 ns for the 500-MHz data and 0.17 ns for the 600-MHz data, whereas the standard deviation is 0.3 ns. The data recorded at 20, 34, and 40°C also exhibited no sign of exchange contributions (data not shown). These findings are surprising given the fact that shortened $T_2$ values are observed for some residues, suggesting the presence of considerable chemical exchange.

The ratio $\eta/R_2$ is independent of internal motions and anisotropy when the high-frequency contributions of the spectral density function to $R_2$ can be neglected; i.e., $J(\omega_H) \ll J(0)$. This can be tested by calculating $J(\omega_H)$ from $T_1$ and heteronuclear NOE using the reduced spectral density approach (*20*). For segment 4 all structured residues (1–100) possess $J(\omega_H)$ values more than two orders of magnitude smaller than the corresponding $J(0)$. In the absence of exchange broadening $\eta/R_2$ then only depends on the magnitude and orientation of the $^{15}N$ CSA tensor, i.e., on $(\sigma_\parallel - \sigma_\perp)$ and cos $\theta$. Figure 3 shows $\eta/R_2$ for the measurements at 500 and 600 MHz at 31°C. The $\eta/R_2$ values obtained from data recorded at 20, 31, 34, and 40°C at a proton frequency of 500 MHz are very similar and therefore only $\eta/R_2$ at one temperature (31°C) is shown. The $\eta/R_2$ ratios obtained from the 600-MHz spectra are of course higher. The mean value of $\eta/R_2$ at 500 MHz is 0.644 with a standard deviation of 7% for residues in $\beta$-strands and 0.629 $\pm$ 9% over the folded part of the protein (residues 1–100). Assuming that $\theta = 20°$ the mean CSA value for $\beta$-strands of segment 4 is $-163$ ppm. The variation in $\eta/R_2$ shows that the CSA tensor is not the same for all residues, but does not vary dramatically, in agreement with recent studies (*14, 17*).

We tried also to determine $(\sigma_\parallel - \sigma_\perp)$ and $\theta$ of the $^{15}N$ chemical shift tensor separately from our data at two field strengths (*18*). This was not possible because our $\eta/R_2$ ratios at 600 MHz were 17% larger than the ratios from the 500-MHz data for $\beta$-sheet residues whereas the theoretical value is 11%. Additional measurements at 500 MHz, using different $^{15}N$ carrier frequencies and $T_{1\rho}$ experiments (data not shown), lead to the conclusion that imperfections of the CPMG sequence used in the $T_2$ experiments cause an additional, systematic error in $T_2$ values of about 5%. This shows again that highly precise data ($\sim$1–2% statistical error in $T_1$ and $T_2$ values) may not necessarily have the same accuracy. Unfortunately determination of $(\sigma_\parallel - \sigma_\perp)$ and $\theta$ of the $^{15}N$ chemical shift tensor from data at different field strengths is quite sensitive to errors in the $\eta/R_2$ ratios so that no values could be obtained for the present case. Still, the relative variation with sequence can be estimated. This is important for the extraction of the anisotropy factor $\sigma$ which is defined as the ratio of the two principal values of the diffusion tensor that we assume to be axially symmetric. From the highest and lowest $J^{cc}(0)$ values for residues that exhibit no internal motions (NOE $> 0.6$) one gets the ratio $J^{cc}_{min}(0)/J^{cc}_{max}(0)$, where $J^{cc}_{min}(0) = 0.3\tau_1 + 0.1\tau_3$ and $J^{cc}_{max}(0) =$

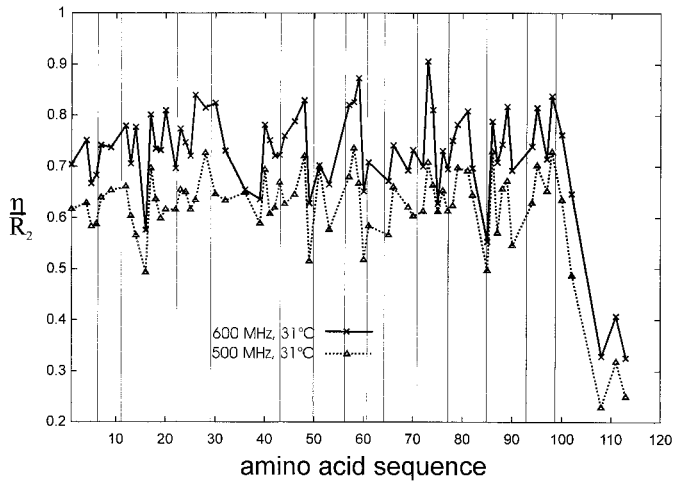


**FIG. 3.** The ratio $\eta/R_2$ is plotted vs amino acid number for measurements at 500 and 600 MHz proton frequency at 31°C. The $\beta$-sheets of segment 4 are indicated by the shaded bars.

**TABLE 1**
**Anisotropy Factors Obtained from Fitting the Diffusion Tensor to Synthetic Data Sets**

| | | Rigid[a] | | Tightly packed[b] | | Flexible[c] | |
|---|---|---|---|---|---|---|---|
| $\sigma$[d] | Data used | ∅ ± SD[e] | #[f] | ∅ ± SD[e] | #[f] | ∅ ± SD[e] | #[f] |
| | | | | 5% Gaussian noise | | | |
| | All | 1.46 ± 0.05 | | 1.40 ± 0.15 | | 1.17 ± 0.19 | |
| 1.5 | | | 79 | | 58 | | 50 |
| | 500 MHz | 1.41 ± 0.05 | | 1.39 ± 0.14 | | 1.18 ± 0.17 | |
| | All | 1.94 ± 0.07 | | 1.79 ± 0.20 | | 1.33 ± 0.17 | |
| 2 | | | 78 | | 57 | | 43 |
| | 500 MHz | 1.84 ± 0.08 | | 1.76 ± 0.19 | | 1.35 ± 0.16 | |
| | All | 3.78 ± 0.15 | | 2.95 ± 0.40 | | 1.93 ± 0.44 | |
| 4 | | | 52 | | 36 | | 10 |
| | 500 MHz | 3.60 ± 0.18 | | 2.85 ± 0.43 | | 1.98 ± 0.34 | |
| | | | | Noise free | | | |
| | All | 1.50 ± 0.01 | | 1.39 ± 0.17 | | 1.17 ± 0.23 | |
| 1.5 | | | 78 | | 59 | | 53 |
| | 500 MHz | 1.50 ± 0.01 | | 1.39 ± 0.14 | | 1.19 ± 0.21 | |
| | All | 1.94 ± 0.06 | | 1.74 ± 0.20 | | 1.29 ± 0.18 | |
| 2 | | | 77 | | 58 | | 45 |
| | 500 MHz | 1.94 ± 0.05 | | 1.73 ± 0.18 | | 1.30 ± 0.16 | |
| | All | 3.83 ± 0.10 | | 2.91 ± 0.30 | | 2.01 ± 0.25 | |
| 4 | | | 51 | | 36 | | 11 |
| | 500 MHz | 3.88 ± 0.07 | | 2.83 ± 0.29 | | 2.03 ± 0.23 | |

*Note.* From 10,000 simulated residues "rigid" residues were identified using the criterion of Tjandra *et al.* (*25*) and divided into subsets of 100 "rigid" residues each. Listed are the average value and standard deviation of the anisotropy factor for all subsets of each data set. See also text.

[a] Lipari–Szabo parameters were generated randomly in the following ranges: $0.5 < S^2 < 0.9$, $0 < \tau_i < 0.7$ ns, $0 < R_{ex} < 1$ Hz. A strong bias toward $S^2 = 0.9$, $\tau_i = 0$, $R_{ex} = 0$ was used for the "rigid" class. For details see Experimental.

[b] As before, but $0.1 < S^2 < 0.9$, $0 < \tau_i < 7$ ns, $0 < R_{ex} < 10$ Hz. Still a bias toward $S^2 = 0.9$, $\tau_i = 0$, $R_{ex} = 0$ was used for the "tightly packed" class.

[c] As before, but parameters were generated without bias in the given ranges.

[d] The anisotropy factor was used in the generation of the synthetic data.

[e] Mean and standard deviation of the back-calculated anisotropy factor over all subsets of one data set.

[f] Number of subsets obtained for one data set = percentage of residues identified as "rigid" by the criterion of Tjandra *et al.* (*25*).

$0.4\tau_3$ in the absence of internal motion (*21*). With $\tau_1 = 6\tau_3/(2 + 4\sigma)$ the anisotropy factor $\sigma$ is given by

$$\sigma = \frac{9}{8J^{cc}_{min}(0)/J^{cc}_{max}(0) - 2} - \frac{1}{2}. \qquad [3]$$

Internal motions reduce the $J^{cc}(0)$ value and therefore present no problem for the determination of $J^{cc}_{max}(0)$. For $J^{cc}_{min}(0)$, on the other hand, too small values might be obtained when residues exhibiting internal motions are not properly recognized. This procedure is similar to the one proposed by Clore *et al.* (*22*) with the difference that exchange broadening cannot affect the resulting anisotropy $\sigma$. Estimating $\sigma$ from $\tau_{min}/\tau_{max} = J_{min}(0)/J_{max}(0)$ ratios has already been proposed by Schurr *et al.* (*23*) in the context of testing the performance of the Lipari–Szabo model.

The rationale for developing our procedure for estimation of the anisotropy factor $\sigma$ was that computer simulations described below showed that the commonly used method of fitting the diffusion tensor to $T_1/T_2$ ratios for residues assumed to be rigid tends to underestimate $\sigma$. Different synthetic data sets consisting of $T_1$, $T_2$, and NOE at 500, 600, and 750 MHz for 10,000 virtual residues were generated randomly with an anisotropic Lipari–Szabo model (*6, 7, 24*) with different exchange contributions using a constant overall correlation time $\tau_3$ of 7.0 ns. Three different anisotropy factors $\sigma = 1.5$, 2.0, and 4.0 and three different degrees of flexibility (rigid, tightly packed, and flexible; Table 1) were investigated with and without 5% Gaussian noise added to the data and are listed in Table 1 (see also Experimental). The criterion of Tjandra *et al.* (*25*) (applied to the 500-MHz NOE and $T_1/T_2$) was used to determine "rigid" residues when fitting the diffusion tensor to the synthetic data. The diffusion tensor was always assumed to be axially symmetric. For each virtual residue the data simulated at 500, 600, and 750 MHz were fit simultaneously and in a separate fit only 500-MHz data were considered. For all data

sets all 10,000 virtual residues were used together for one fitting procedure whereas in a second fit all "rigid" residues were divided into subsets of 100 residues each. For each subset an anisotropy factor $\sigma$ was determined independently. An average value, as well as the standard deviation of $\sigma$ over all subsets of one data set, is listed in Table 1. In all cases the difference between the $\sigma$'s resulting from the first and second calculations was smaller than 0.1 and therefore the results from the first calculation are not shown in Table 1 and are disregarded in the further discussion.

For each of the nine data sets four different fitting procedures were performed, resulting in 12 different back-calculated anisotropy parameters $\sigma$ for each of the three original $\sigma$'s (1.5, 2.0, 4.0) showing the dependence of the resulting $\sigma$ on flexibility, experimental uncertainty, and amount of data available. The correct anisotropy is obtained only when the order parameter is restricted to high values and exchange contributions are negligible. As soon as internal motions and exchange broadening are included the results for the anisotropy $\sigma$ are too low. Relaxation rates of 10,000 (virtual) residues (at three field strengths) were used in the grid search for the optimum $\sigma$. Therefore insufficient sampling of the unit sphere by the N–H bond directions or bad statistics cannot possibly account for the difference between back-calculated and original anisotropy. We performed additional simulations where either $\tau_i$ or $R_{ex}$ was set to zero, in order to identify which motions are responsible for the observed underestimation of the anisotropy $\sigma$ (data not shown). For the "tightly packed" class setting $\tau_i$ to zero had almost no influence on the back-calculated anisotropy factors; only the number of residues identified as rigid by the criterion of Tjandra *et al.* (*25*) increased. Quite differently, with $R_{ex} = 0$ the original anisotropy factors could be reproduced very well, even for $\sigma = 4.0$. For the "flexible" class neither $\tau_i = 0$ nor $R_{ex} = 0$ could reproduce the original anisotropy and both seem to contribute approximately equally to the underestimation observed (Table 1). This shows that for small amounts of internal motions only chemical exchange presents a problem, whereas for larger flexibility both fast and slow internal motions lead to similar degrees of underestimation of the anisotropy factor.

Using the fitting procedure of Tjandra *et al.* (*25*) with its statistical criterion for identifying exchange broadening on our experimental data for segment 4 of the gelation factor from one or two field strengths did not yield significant anisotropy ($\sigma = 1.1$ for all temperatures and also for 500- and 600-MHz data at 31°C simultaneously) although from the structure (*19*) an anisotropy factor of $\sigma = 1.9$ was calculated using the method described in (*24*) (excluding the disordered C-terminus). The inertia tensor of segment 4 has eigenvalues in the ratio 1:0.97:0.29 so that we do not anticipate appreciable rhombicity for the diffusion tensor and assume therefore axial symmetry. If a (too low) anisotropy factor of $\sigma = 1.1$ is used in the relaxation analysis artificial exchange contributions are found. This has already been observed (*9*).

Recently, we have investigated the dynamics of the CDK inhibitor $p19^{INK4d}$ (*26*). The protein consists mainly of $\alpha$-helix bundles with all $\alpha$-helices orthogonal to the symmetry axis of the diffusion tensor (*27*). Despite an inertia tensor with principal values in the ratio 1:0.88:0.34 no anisotropy is found by the fitting procedure ($\sigma = 1.0$ or 1.1 for data from one or two field strengths). However, in our study incorporation of anisotropy into the analysis was crucial for interpretation, especially with regard to CDK binding (*26*).

When determining the $J^{cc}_{min}(0)/J^{cc}_{max}(0)$ ratio one must consider not only the uncertainty of the $\eta$ and $J(\omega_N)$ values, but also the variation of $c/(c^2 + d^2)P_2(\cos\theta)$ over the sequence. In the present case $J^{cc}_{max}(0) \approx 3.8$ ns, and $J^{cc}_{min}(0) \approx 2.2$ ns can be estimated from Fig. 2A with errors of ca. 4% due to uncertainties in the $\eta$ and $J(\omega_N)$ values and ca. 9% due to variations of $c/(c^2 + d^2)P_2(\cos\theta)$. This translates to a $J^{cc}_{min}(0)/J^{cc}_{max}(0)$ ratio of $0.58 \pm 0.08$ which corresponds to an anisotropy factor $\sigma = 2.9$, $2.1 < \sigma < 4.0$. As $\sigma \to \infty$ for $J^{cc}_{min}(0)/J^{cc}_{max}(0) \to \frac{1}{4}$ it is apparent that for large amounts of anisotropy error propagation from $J^{cc}_{min}(0)/J^{cc}_{max}(0)$ ratios to anisotropy factors $\sigma$ becomes increasingly unfavorable. In many cases it might thus be preferable to determine $\sigma$ from the $J_{min}(0)/J_{max}(0)$ ratio using $J^{cc}(0)$ to exclude residues exhibiting exchange contributions. $J_{min}(0)/J_{max}(0)$ is much less sensitive to variations in the $^{15}N$ CSA tensor and does not depend on $J(\omega_N)$. The uncertainty in $J(0)$ is dominated by the experimental error in $T_2$ values. A disadvantage of $J(0)$ is that possible errors introduced by the CPMG sequence might affect $J_{min}(0)/J_{max}(0)$, whereas the cross-correlation experiment does not need any such multipulse sequence during the build-up time of the cross-correlation peaks. For segment 4 $J_{max}(0)$ is 3.5 ns and $J_{min}(0) \approx 2.0$ ns. As the CSA contribution to $T_2$ relaxation is smaller than 20% at 500 MHz the variation of the $^{15}N$ CSA tensor contributes only an uncertainty of 2% in the $J_{min}(0)/J_{max}(0)$ ratio. Disregarding possible errors induced by the CPMG sequence the experimental error of $T_2$ values is <2%. $J_{min}(0)/J_{max}(0)$ is equal to $0.57 \pm 0.02$ and therefore $\sigma = 3.0 \pm 0.25$. Including a possible 5% error from the CPMG one obtains for the anisotropy factor $\sigma = 3.0 \pm 0.6$.

The estimated anisotropy factors are unexpectedly high and exceed the value $\sigma = 1.9$ calculated from the structure of the folded part of segment 4 (residues 1–100) by far. However, looking at an NMR-derived family of structures, including the last 22 unstructured residues, one finds that for all structures of the family the C-terminal tail prolongs the shape of the molecule. Including the flexible C-terminus one calculates from the family of structures an anisotropy factor $\sigma = 3.1 \pm 0.6$ using the protocol described in (*24*). This agrees well with our results derived from cross-correlation rates. Thus we find that for the segment 4 construct only the flexible C-terminal tail can explain the observed anisotropy. This is different from the case described by Tjandra *et al.* (*25*) where the authors found that agreement between the structure-derived diffusion tensor and a diffusion tensor obtained by fitting $T_1/T_2$ ratios was achieved

as well by ignoring an unstructured terminal tail as by averaging over an ensemble of structures. However, the flexible tail was much shorter in their case.

## DISCUSSION AND CONCLUSIONS

Our extensive computer simulations show that in general the current common procedure of fitting the diffusion tensor to experimental $T_1/T_2$ ratios underestimates the anisotropy of the rotational diffusion. The reason for this lies in selection criteria that exclude residues on a statistical basis (see Computer simulations under Experimental). These criteria assume implicitly that for every residue that exhibits internal motion or exchange broadening there are at least two rigid residues *with N–H bond vectors pointing (approximately) in the same direction.* In the case of folded proteins this might be taken for granted for $\alpha \approx 90°$. But for residues with $\alpha \approx 0°$ the distinction between exchange broadening and anisotropic effects is crucial as the probability of N–H vectors being parallel to the symmetry axis of the diffusion tensor is much smaller than that of being orthogonal (this probability is proportional to the sine of the angle between the N–H vector and the symmetry axis). When using prevailing statistical criteria to identify exchange broadening the small number of N–H vectors parallel to the symmetry axis is likely to be excluded on the basis of their exceptional short $T_2$ times. Indeed, we found for two definitely anisotropic proteins, one being segment 4 of the gelation factor built exclusively from $\beta$-sheets and the other the CDK inhibitor $p19^{INK4d}$, consisting mainly of $\alpha$-helix bundles, that the fitting procedure yielded only negligible anisotropy ($\sigma = 1.1$ in both cases). This was because the N–H bond vector directions are clustered in $\alpha$-helices and $\beta$-strands.

It has been shown by Tjandra *et al.* (*9*) that inaccurate anisotropy factors lead to incorrect values for the $R_{ex}$ parameter within the Lipari–Szabo model. Our approach circumvents these problems by separating exchange contributions and effects of anisotropy with the help of cross-correlation rates which contain information about anisotropy but are free from exchange contributions. Exchange broadening and the anisotropy factor are determined independently whence uncertainties in one value (e.g., the anisotropy factor) do not influence the other (the exchange contribution). Also, similarly to the approach of Clore *et al.* (*22*), detailed structural information is not needed, as long as axial symmetry can be assumed for the diffusion tensor.

The application of our approach to segment 4 has shown that the anisotropy factor cannot be determined to high accuracy. This does not present a problem because Lipari–Szabo order parameters $S^2$ are quite insensitive to the exact amount of anisotropy present (*9, 23*). The sensitivity of the exchange parameter $R_{ex}$ in the Lipari–Szabo model to changes in the anisotropy factor $\sigma$ is immaterial because exchange broadening is detected from a comparison of $J(0)$ and $J^{cc}(0)$ in our approach.

In conclusion, we believe that the measurement of cross-correlation rates between $^{15}N$ CSA and $^{15}N$–$^{1}H$ dipole–dipole relaxation and subsequent application of the approach presented here can provide valuable information for almost every $^{15}N$ relaxation study.

## EXPERIMENTAL

All NMR experiments were carried out on Bruker DRX500 and DRX600 spectrometers equipped with PFG accessories on a 1.5 mM uniform $^{15}N$-labeled sample of segment 4 of the gelation factor (ABP 120) in 90% $H_2O$/10% $D_2O$ at pH 7.0. The construct of the gelation factor used in our study comprises 122 residues (*19*). Residues 1–100 are folded and constitute the proper fourth segment of the rod domain of the gelation factor. The C-terminal 22 residues are unfolded as seen from NOE measurements (*19*). The complete set of $T_1$, $T_2$, and NOE was recorded at 20, 31, 34, and 40°C at 500 MHz proton frequency and at 600 MHz proton frequency at 31°C. Modified versions of the experiments proposed by Farrow *et al.* (*8*), where water suppression was achieved by the WATERGATE sequence (*28*) rather than by gradient-pathway selection, were used for $T_1$, $T_2$, and NOE measurements. In the $T_1$ and $T_2$ experiments water saturation was avoided by using low-power water-flipback pulses. Following the guidelines of (*29*) relaxation periods of 16 ms + $x$ * 32 ms for $T_2$ and 11 ms + 220 ms * $x$ for $T_1$ with $x = 0, 1, 2, 3, 4$ were used. Saturation of the amide protons in the heteronuclear NOE experiment was achieved by the application of a series of 120° pulses prior to the experiment (*30*). Table 2 shows average values for all $T_1$, $T_2$, and NOE experiments. Two different experiments were used to determine cross-correlation rates. The experiment proposed by Tjandra *et al.* (*14*) was performed as described by the authors whereas in the experiment of Tessari *et al.* (*15*) the gradient-selection sensitivity-enhancement scheme was replaced by the simple WATERGATE sequence (*28*). In the experiment of Tessari *et al.* (*15*) the phase cycle as given in the paper is not correct: the receiver phase should be cycled ($P$, $-P$, $-P$, $P$) with $P = (x, -x, -x, x)$ not ($2P$, $4(-P)$, $2P$) as given in the publication. The relaxation delays used for the cross-correlation experiments are summarized in Table 3. For all experiments at least 140 ($^{15}N$) times 2048 ($^{1}H$) data points were acquired with spectral widths of 35 ppm ($^{15}N$) and 11 ppm ($^{1}H$). Most experiments were recorded in an interleaved manner to reduce influence from possible instabilities in experimental conditions.

NOE values are given simply by the ratio of the peak heights in the experiment with and without proton saturation. To obtain $T_1$ and $T_2$ values, the experimental data points (peak heights) were fit to a curve $A \exp(-t/T_{1or2})$ with a simple grid search. Uncertainties were determined from double recording either of single data points or of the whole relaxation experiment.

For the cross-correlation rates $\eta$ the ratios of signal intensities (peak heights) from the cross-correlation experiment and

**TABLE 2**
**Mean Values, Standard Deviation, and Average Error of Experimental Relaxation Rates for the Folded Part (Residues 1–100) of Segment 4**

| | 20°C | | | 31°C | | | 34°C | | | 40°C | | | 31°C, 600 MHz | | |
|---|---|---|---|---|---|---|---|---|---|---|---|---|---|---|---|
| | Mean | SD[b] | Error[c] | Mean | SD[b] | Error[c] | Mean | SD[b] | Error[c] | Mean | SD[b] | Error[c] | Mean | SD[b] | Error[c] |
| $T_1$ [ms] | 584 | 80 | 0.6[a] | 480 | 56 | 1.2[a] | 452 | 52 | 0.6 | 418 | 45 | 1.8 | 590 | 77 | 3.0[a] |
| $T_2$ [ms] | 83.7 | 11.3 | 0.8[a] | 110.8 | 13 | 1.1 | 117.3 | 13.7 | 0.8 | 131.6 | 15.3 | 1.4 | 104 | 12.4 | 0.4[a] |
| NOE | 0.712 | 0.077 | 1.4 | 0.692 | 0.07 | 2.0[a] | 0.709 | 0.06 | 1.6 | 0.599 | 0.058 | 1.5 | 0.75 | 0.07 | 7.0[a] |
| CC2[d] [Hz] | — | — | — | 5.74 | 0.96 | 1.7[a] | 5.27 | 0.84 | 1.4[a] | 4.71 | 0.73 | 1.5 | 7.16 | 1.28 | 2.1[a] |
| CC1[e] [Hz] | 6.02 | 0.84 | 1.6[a] | — | — | — | 5.2 | 0.68 | 1.5 | 4.58 | 0.66 | 1.8[a] | 6.77 | 0.91 | 2.3[a] |

*Note.* Unless otherwise indicated all data were extracted from spectra recorded at 500 MHz proton frequency.
[a] Error [%] estimated from double recording of one data point; for cross-correlation experiments this means that only the (more sensitive) reference experiment was not recorded twice.
[b] Standard deviation.
[c] Average error [%] for residues 1–100; calculated as root mean square difference between two identical experiments (except for values marked with superscript *a*).
[d] Cross-correlation rate measured with a modified version of the experiment proposed by Tessari *et al.* (*15*).
[e] Cross-correlation rate measured with the experiment proposed by Tjandra *et al.* (*14*).

the corresponding reference experiment were fit either to a curve $A \tanh(T\eta)$ (*14*) or to a simple linear relation $T\eta$ (*15*). In both experiments, one 2D experiment contains only cross peaks from cross-correlation between $^{15}$N CSA and $^{15}$N–$^{1}$H dipole–dipole relaxation whereas a second slightly modified 2D experiment serves as a reference. All rates were extracted from spectra recorded in an interleaved manner so that spectrometer instabilities would not affect the experiment and reference measurements differently. For each $t_1$ increment, the cross-correlation experiment was run twice, followed by one reference increment, so that finally two 2D cross-correlation experiments and one reference experiment were obtained. Although this mode of recording was dictated by the two to three times higher sensitivity of the reference experiment (compared to the cross-correlation experiment) and the inability of current pulse program syntax to record experiments with different numbers of scans within one pulse program, it has the advantage that reproducibility of the data can be computed as rmsd between the two spectra recorded with identical setups. Sixty-eight peaks were well resolved at all four temperatures, so that $T_1$, $T_2$, NOE, and cross-correlation rates could be obtained.

**TABLE 3**
**Build-Up Times Used in the Cross-Correlation Experiments**

| Experiment | Tessari *et al.* (*15*) | Tjandra *et al.* (*14*) |
|---|---|---|
| 20°C at 500 MHz | — | 60 ms (2×), 100 ms |
| 31°C at 500 MHz | 60 ms | — |
| 34°C at 500 MHz | 40 ms, 60 ms, 80 ms, 160 ms | 60 ms (2×), 100 ms, 160 ms |
| 40°C at 500 MHz | 60 ms (2×), 100 ms | 60 ms (2×), 100 ms |
| 31°C at 600 MHz | 60 ms | 60 ms |

*Note.* Multiple recordings are indicated in parentheses.

*Reduced spectral density mapping.* The spectral density function $J(\omega)$ has small values for $\omega = \omega_H$ ($^1$H angular spin precession frequency) as shown by Peng and Wagner (*31, 32*) and Lefèvre *et al.* (*33*). Therefore, it can be assumed that it varies only little in the vicinity of $\omega_H$. For $\omega = \omega_H \pm \omega_N$ we used the approximation $J(\omega) \propto 1/\omega^2$ of (*20*). Values of $J(\omega)$ can thus be calculated at $\omega = \omega_0$, $\omega_N$, 0.870 $\omega_H$ from $T_1$, $T_2$, and NOE data (*20*).

*Computer simulations.* Synthetic data sets of $T_1$, $T_2$, and NOE at 500, 600, and 750 MHz for 10,000 virtual residues were generated randomly as follows. From homogeneously distributed random numbers $X \in [0, 1]$ ($P(X) = \text{const.}$), the order parameter $S^2$, the internal correlation time $\tau_i$, and an exchange contribution $R_{ex}$ was calculated for each virtual residue with the formulas given below. Assuming an axially symmetric diffusion tensor the following anisotropic Lipari–Szabo model (*21, 24*) with a constant overall correlation time $\tau_3$ of 7.0 ns was used to generate spectral densities $J(\omega)$:

$$J(\omega) = \frac{2}{5}\left(A_1 \frac{\tau_1}{1 + \omega^2\tau_1^2} + A_2 \frac{\tau_2}{1 + \omega^2\tau_2^2} + A_3 \frac{\tau_3}{1 + \omega^2\tau_3^2}\right) \times S^2 + \frac{2}{5}\frac{\tau}{1 + \omega^2\tau_{eff}^2}(1 - S^2). \quad [4]$$

The coefficients $A_i$ and correlations times $\tau_i$ are calculated from $\tau_3$ and the angle $\alpha$ between the N–H bond vector and the symmetry axis of the diffusion tensor as $A_1 = 0.75 \sin^4\alpha$, $A_2 = 3 \sin^2\alpha \cos^2\alpha$, $A_3 = (1.5 \cos^2\alpha - 0.5)^2$, $\tau_1 = 6\tau_3/(2 + 4\sigma)$, and $\tau_2 = 6\tau_3/(5 + \sigma)$. The parameter $\sigma$ is a measure of the anisotropy and is defined as the ratio of the two eigenvalues of the diffusion tensor $\sigma = D_\parallel/D_\perp$. The effective internal correlation time $\tau_{eff}$ is given by $\tau_{eff}^{-1} = 3/(\tau_1 + \tau_2 + \tau_3) + \tau_i^{-1}$. For

every virtual residue the angle $\alpha$ is also generated randomly as $\cos^2\alpha = X^2$ according to a homogeneous distribution of N–H vectors over the sphere. No errors in the $\cos^2\alpha$ values were introduced thereby disregarding an important source of error for real cases. Synthetic data sets were created for three different degrees of anisotropy $\sigma = 1.5, 2.0, 4.0$. For each different degree of anisotropy $\sigma$ Lipari–Szabo parameters were calculated from the random numbers $X \in [0, 1]$ in three different ways classified as rigid ($S^2 = 0.9 - 0.4 * X^4$, $\tau_i = 0.7 * X * 10^{3X}$ ps, $R_{ex} = 10^{4*X-4}$ Hz), tightly packed ($S^2 = 0.9 - 0.8 * X^2$, $\tau_i = 0.7 * X * 10^{4X}$ ps, $R_{ex} = X^2 * 10$ Hz), and flexible ($S^2 = 0.9 - 0.8\ X$, $\tau_i = X * 7.0$ ns, $R_{ex} = X * 10$ Hz) to mimic residues in rigid secondary structure elements, in well-ordered structures with little flexibility and in highly mobile regions, respectively. The bias toward $S^2 = 0.9$, $\tau_i \ll \tau_3$, $R_{ex} = 0$, is very strong for the rigid class and still strong for the tightly packed class. The flexible class on the other hand is generated with unbiased (within reasonable bounds) linearly distributed parameter values. From the spectral densities obtained by Eq. [4] $T_1$, $T_2$, and NOE at magnetic field strengths of 500, 600, and 750 MHz were calculated with well-known formulas (e.g., *8, 12, 13, 20, 24, 31–33*). Altogether nine data sets comprising $T_1$, $T_2$, and NOE values at three field strengths for 10,000 residues each were generated and investigated. From the synthetic data sets the anisotropy parameter $\sigma$ was calculated in several different ways, all based on the procedure described by Tjandra *et al.* (*25*). Briefly this procedure consists of a criterion identifying rigid residues and subsequent fitting of the diffusion tensor to the experimental $T_1/T_2$ ratios. Commonly used criteria require the NOE to exceed some threshold (0.6–0.7) and exclude residues with unusual $T_1$ and/or $T_2$ values in a statistical way; e.g., in (*25*) residues with $T_1/\langle T_1\rangle - T_2/\langle T_2\rangle > 1.5$ SD are excluded, where $\langle\ \rangle$ denotes the average over all residues with NOE $> 0.6$ and SD is the standard deviation of $T_1/\langle T_1\rangle - T_2/\langle T_2\rangle$ for the same residues. The back-calculation of $\sigma$ was performed for every data set with and without 5% Gaussian noise added to the $T_1$, $T_2$, and NOE values. Also either data from all field strengths were used in the fitting or only the 500-MHz $T_1/T_2$ ratios were considered. Each fitting procedure was performed in two ways: In one all rigid residues (of the 10,000) were used simultaneously for fitting and in the other the rigid residues were divided into subsets of 100 and fitting was performed separately for each subset. In the latter case the resulting anisotropy factors $\sigma$ from all subsets were averaged and a standard deviation was calculated. Therefore eight different fitting procedures were performed for each of the nine data sets.

Additional simulations were performed as described above with the modification that data sets were generated either with $\tau_i$ or with $R_{ex}$ set to zero. From these data sets anisotropy factors were also back-calculated to distinguish between the effects of fast and slow internal motions on the calculated anisotropy.

*Supporting information.* Five tables containing $T_1$, $T_2$, NOE, and cross-correlation rates of segment 4 at 20, 31, 34, and 40°C from 500-MHz spectra and at 31°C from 600-MHz spectra are available from the authors and were submitted to the Indiana Dynamics Database (www:pooh.chem.indiana.edu/IDD.html).

## ACKNOWLEDGMENTS

We thank Paola Fucini for the gift of the $^{15}$N sample of segment 4 of the gelation factor (ABP-120). This work was supported by a DFG grant (SFB 413).

## REFERENCES

1. K. T. Dayie, G. Wagner, and J.-F. Lefèvre, Heteronuclear relaxation and the experimental determination of the spectral density function, *in* "Dynamics and the Problem of Recognition in Biological Macromolecules" (O. Jardetzky and J.-F. Lefèvre, Eds.), NATO ASI Series A, Vol. 288, Plenum Press, New York (1996).
2. L. E. Kay, Protein dynamics from NMR, *Biochem. Cell Biol.* **76,** 145–152 (1998).
3. M. W. F. Fischer, A. Majumdar, and E. R. P. Zuiderweg, Protein NMR relaxation: Theory, applications and outlook, *Prog. NMR Spectrosc.* **33,** 207–272 (1998).
4. A. G. Palmer, *Curr. Opin. Strut. Biol.* **7,** 732–737 (1997).
5. J. P. Loria, M. Rance, and A. G. Palmer, *J. Am. Chem. Soc.* **121,** 2331–2332 (1999).
6. G. Lipari and A. Szabo, Model-free approach to the interpretation of nuclear magnetic resonance relaxation in macromolecules. 1. Theory and range of validity, *J. Am. Chem. Soc.* **104,** 4546–4559 (1982).
7. G. Lipari and A. Szabo, Model-free approach to the interpretation of nuclear magnetic resonance relaxation in macromolecules. 2. Analysis of experimental results, *J. Am. Chem. Soc.* **104,** 4559–4570 (1982).
8. N. A. Farrow, R. Muhandiram, A. U. Singer, S. M. Pascal, C. M. Kay, G. Gish, S. E. Shoelson, T. Pawson, J. D. Foreman-Kay, and L. E. Kay, Backbone dynamics of a free and a phosphopeptide-complexed Src Homology 2 domain studied by $^{15}$N NMR relaxation, *Biochemistry* **33,** 5984–6003 (1994).
9. N. Tjandra, P. Wingfield, S. Stahl, and A. Bax, Anisotropic rotational diffusion of perdeuterated HIV protease from $^{15}$N NMR relaxation measurements at two magnetic fields, *J. Biomol. NMR* **8,** 273–284 (1996).
10. V. Y. Orekhov, K. V. Pervushin, D. M. Korzhnev, and A. S. Arsieniev, Backbone dynamics of (1-71)- and (1-36)bactrioopsin studied by two-dimensional $^1$H–$^{15}$N NMR spectroscopy, *J. Biomol. NMR* **6,** 113–122 (1995).
11. M. Akke and A. G. Palmer III, Monitoring macromolecular motions on microsecond to millisecond time scales by $R_{1\rho}$–$R_1$ constant relaxation time NMR spectroscopy, *J. Am. Chem. Soc.* **118,** 911–912 (1996).
12. I. Q. H. Phan, J. Boyd, and I. D. Campbell, Dynamic studies of a fibronectin type I module pair at three frequencies: Anisotropic modelling and direct determination of conformational exchange, *J. Biomol. NMR* **8,** 369–378 (1996).
13. S. Zinn-Justin, P. Berthault, M. Guenneugues, and H. Desvaux, Off-resonance rf fields in heteronuclear NMR: Application to the study of slow motions, *J. Biomol. NMR* **10,** 363–372 (1997).

14. N. Tjandra, A. Szabo, and A. Bax, Protein backbone dynamics and $^{15}N$ chemical shift anisotropy from quantitative measurement of relaxation interference, *J. Am. Chem. Soc.* **118,** 6986–6991 (1996).
15. M. Tessari, F. A. A. Mulder, R. Boelens, and G. W. Vuister, Determination of amide proton CSA in $^{15}N$-labeled proteins using $^{1}H$ CSA/$^{15}N$–$^{1}H$ dipolar and $^{15}N$ CSA/$^{15}N$–$^{1}H$ dipolar cross-correlation rates, *J. Magn. Reson.* **127,** 128–133 (1997).
16. C. D. Kroenke, J. P. Loria, L. K. Lee, M. Rance, and A. G. Palmer III, Longitudinal and transverse $^{1}H$–$^{15}N$ dipolar/$^{15}N$ chemical shift anisotropy relaxation interference: Unambiguous determination of rotational diffusion tensors and chemical exchange effects in biological macromolecules, *J. Am. Chem. Soc.* **120,** 7905–7915 (1998).
17. D. Fushman and D. Cowburn, Model-independent analysis of $^{15}N$ chemical shift anisotropy from NMR relaxation data. Ubiquitin as a test example, *J. Am. Chem. Soc.* **120,** 7109–7110 (1998).
18. D. Fushman, N. Tjandra, and D. Cowburn, Direct measurement of $^{15}N$ chemical shift anisotropy in solution, *J. Am. Chem. Soc.* **120,** 10947–10952 (1998).
19. P. Fucini, C. Renner, C. Herberholt, A. A. Noegel, and T. A. Holak, The repeating segments of the F-actin crosslinking gelation factor (ABP-120) have an immunoglobulin-like fold, *Nat. Struct. Biol.* **4,** 223–230 (1997).
20. N. A. Farrow, O. Zhang, A. Szabo, D. A. Torchia, and L. E. Kay, Spectral density function mapping using $^{15}N$ relaxation data exclusively, *J. Biomol. NMR* **6,** 153–162 (1995).
21. D. E. Woessner, Nuclear spin relaxation in ellipsoids undergoing rotational Brownian motion, *J. Chem. Phys.* **37,** 647–654 (1962).
22. G. M. Clore, A. M. Gronenborn, A. Szabo, and N. Tjandra, Determining the fully asymmetric diffusion tensor from heteronuclear relaxation data in the absence of structural information, *J. Am. Chem. Soc.* **120,** 4889–4890 (1998).
23. J. M. Schurr, H. P. Babcock, and B. S. Fujimoto, A test of the model-free formulas. Effects of anisotropic rotational diffusion and dimerization, *J. Magn. Reson. B* **105,** 211–224 (1994).
24. T. Zink, A. Ross, K. Lüers, C. Cieslar, R. Rudolph, and T. A. Holak, Structure and dynamics of the human granulocyte colony-stimulating factor determined by NMR spectroscopy. Loop mobility in a four-helix-bundle protein, *Biochemistry* **33,** 8453–8463 (1994).
25. N. Tjandra, S. E. Feller, R. W. Pastor, and A. Bax, Rotational diffusion anisotropy of human ubiquitin from $^{15}N$ NMR relaxation, *J. Am. Chem. Soc.* **117,** 12562–12566 (1995).
26. C. Renner, R. Baumgartner, A. A. Noegel, and T. A. Holak, Backbone dynamics of the CDK inhibitor $p19^{INK4d}$ studied by NMR $^{15}N$ relaxation experiments at two field strength, *J. Mol. Biol.* **283,** 221–229 (1998).
27. R. Baumgartner, C. Fernandez-Catalan, A. Winoto, R. Huber, R. A. Engh, and T. A. Holak, Structure of human cyclin-dependent kinase inhibitor $p19^{INK4d}$: Comparison to known ankyrin-repeat-containing structures and implications for the dysfunction of tumor suppressor $p16^{INK4a}$, *Structure* **6,** 1279–1290 (1998).
28. V. Sklenář, M. Piotto, R. Leppik, and V. Saudek, Gradient-tailored water suppression for $^{1}H$–$^{15}N$ HSQC experiments optimized to retain full sensitivity, *J. Magn. Reson. A* **102,** 241–245 (1993).
29. J. A. Jones, P. Hodgkinson, A. L. Barker, and P. J. Hore, Optimal sampling strategies for the measurement of spin–spin relaxation times, *J. Magn. Reson. B* **113,** 25–34 (1996).
30. J. L. Markley, W. J. Horsley, and M. P. Klein, Spin–lattice relaxation measurements in slowly relaxing complex spectra, *J. Chem. Phys.* **55,** 3604 (1971).
31. J. W. Peng and G. Wagner, Mapping of spectral density functions using heteronuclear NMR relaxation measurements, *J. Magn. Reson.* **98,** 308–332 (1992).
32. J. W. Peng and G. Wagner, Mapping of the spectral densities of N–H bond motions in Eglin c using heteronuclear relaxation experiments, *Biochemistry* **31,** 8571–8586 (1992).
33. J.-F. Lefèvre, K. T. Dayie, J. W. Peng, and G. Wagner, Internal mobility in the partially folded DNA binding and dimerization domains of GAL4: NMR analysis of the N–H spectral density functions, *Biochemistry* **35,** 2674–2686 (1996).